Wear resistance and fracture behavior of thermally sprayed Al-based quasicrystalline composite coatings

Wear resistance and fracture behavior of thermally sprayed Al-based quasicrystalline composite coatings

Meng Xiao [1,2,a], Zhaoguo Qiu[1,2, b], Yaosha Wu[3,c*], Dechang Zeng [1,2,d*]

[1] School of Materials Science and Engineering, South China University of Technology, Guangzhou, 510640, China

[2] Zhongshan R&D Center for Materials Surface and Thin Films Technology of the South China University of Technology, Gent Materials Surface Technology (Guangzhou) Co., Ltd, Zhongshan, 528437, China

[3] Zhongshan Torch Polytechnic, Zhongshan 528436, China

[a]email: 201710103115@mail.scut.edu.cn, [b]email：zgqiu@scut.edu.cn,

Corresponding author: [c]*email：547656588@qq.com,[d] *email：medczeng@scut.edu.cn

Abstract: Tailoring coating microstructure and the fraction of quasicrystalline phase for enhancing the wear and crack resistance by selecting the appropriate thermal spraying parameters was investigated. To simplify the optimization process, orthogonal test was introduced. According to the statistical analysis and validation experiments, the orders of spraying-parameters that affected the hardness and fraction of quasicrystalline phase were proposed, respectively. The wear resistance and fracture behaviors of coating sprayed with optimal processing parameters were analyzed by pin-on-disk and three-point bending (3PB) tests. The current results indicated that the coating sprayed with optimal parameters exhibit a better wear and crack resistance. The high fraction of quasicrystal phase and dense microstructure contribute to the good wear resistance, meanwhile, the favorable fracture toughness is attributed to the tough phase existing in quasicrystal matrix and a fine-lamellar microstructure which facilitates the stress release during the crack propagation. This study gives insight into the crack propagation behavior in Al-based quasicrystal coating from nano-scale to micro-scale and might provide a viable guideline for the improvement of wear and crack resistance for thermal spraying quasicrystal composite coatings.

1. Introduction

The quasicrystallines (QCs) display attractive properties, such as high hardness, low thermal conductivity, high corrosion and wear sistance [1, 2]. In spite of their outstanding properties, the room temperature brittleness has hindered the applications of quasicrystals in bulk form. The plastic deformation only occurred at high temperatures for bulk material [3] or at sub-micrometer scale for samples at room temperature [4]. In order to solve this problem, fabricating QC coatings via thermal spraying techniques for wear and corrosion applications have aroused increasing attention.

Among various thermal spraying techniques, including plasma spraying, high velocity oxygen fuel (HVOF) and high velocity air fuel (HVAF), the HVAF process, which relies more on kinetic energy than on thermal energy [5], indeed allows feedstock to obtain higher particle velocities, higher powder feeding rate, lower temperature and less oxidizing atmosphere [6]. Moreover, in M3 HVAF torch, high pressure capabilities and total replacement of oxygen with air together with later developments of the

combustion chamber design significantly improved the deposition efficiency and wear and corrosion properties of coatings in contrast with the HVOF [7]. However, on the one hand, element loss and initial phase change are inevitable during the in-flight process for the starting powder [8, 9]. For QCs, Al element loss by vaporization and/or severe particle oxidation resulted in the formation of cubic β-Al(Fe,Cu) phase at the expense of QC phase，especially for fine powder [10], meanwhile, the brittle phase together with tensile residual stresses can result in crack formation [7]. In the development of Al-based QC coatings, the maximum fraction of the QC phase and low porosity are desired for enhancing the wear and corrosion resistance of coatings [11, 12]. On the other hand, during the thermal spraying process, coating porosity inevitably exists at lamellar intersplat due to uncompleted splats contact, unmelted particles and thermal stress [13]. Moreover, oxides form in the periphery of porosity defects, thus deteriorate the stability of passive film during corrosion process [8]. Therefore, the investigation of the effects of microstructure and phase content on the wear and crack resistance is also important. In general, tailoring of the coating properties is mainly achieved by changing the feedstock material type and composition, and by selecting an appropriate thermal spray process. These three aspects affected the temperature, velocity and flying time of in-flight the particles [14] and further controlled the deformation behaviors of splats [15].

As reported by our previous work [16], the optimal particle size of $Al_{65}Cu_{20}Fe_{10}Cr_5$ was determined as +12–49 μm. Therefore, in this work, a series of HVAF sprayed Al-based QC coatings has been fabricated by different the processing parameters, aiming at adjusting the final phases, minimizing the porosity or cracks. In general, a detail research based on a single variant is designed to investigate the effect of related parameters on the final properties of material, which is a very time-consuming due to a lot of experiments. Orthogonal test can shorten the studied period by investigating the multiple factors simultaneously. Therefore, in this paper, effects of the spray distance, fuel pressure and feed rate of particle on the properties of HVAF-sprayed QCs coating are researched by orthogonal test method. Besides, the wear resistance and fracture behavior of coating sprayed with optimal processing parameters were analyzed by pin-on-disk and three-point bending (3PB) tests.

2. Experimental process

2.1. Material and Coating deposition process

Commercial gas-atomized powders of atomic compositions $Al_{65}Cu_{20}Fe_{10}Cr_5$ were employed as feedstock. Laser diffraction system (Better size 2000LD) was used for analysis size distribution. Medium carbon steel with dimensions of 60 × 50 × 5 mm^3 was used as substrate. Prior to the spray process, the substrate was sandblasted for enhancing the bonding strength. Then, the coatings were sprayed by HVAF spray system (Unique Coat Technologies M3™), in which the propane, designated as fuel 1 and fuel 2, were injected into combustion chamber and secondary extension nozzle with additional air simultaneously. Fig. 1 shows the schematic representation of HVAF torch and deposition process, in which the fuel pressure, spray distance and powder feed rate were settled at various values for spraying-parameters optimization.

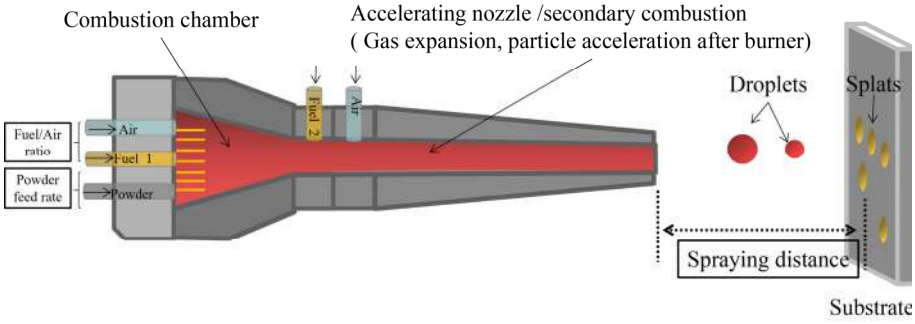

Fig. 1 The schematic representation of HVAF torch and deposition process

2.2. Orthogonal test design

The orthogonal test method was introduced to investigate three factors, including spray distance (marked as A), fuel 1 pressure (marked as B) and feed rate of particle (marked as C). Factors and levels for orthogonal test design are listed in Table 1. To compare the obtained results under different conditions, the parameter R is introduced to quantify the difference of microhardness and fraction of i-QC phase for various coatings.

$$R = K_{AVi}^{max} - K_{AVi}^{min} \quad (1)$$

where K_{AVi}^{max} and K_{AVi}^{min} represent the maximum and minimum average value of microhardness for one level of a factor. If the R value is larger, the level change for the factor has a greater effect on the properties of coating.

2.3. Characterization and properties tests

The phases and morphology of the powder and coatings were characterized by X-ray diffraction (XRD, Philips X-Pert Pro, Cu Kα1 radiation) and scanning electron microscopy (SEM, Nova Nano SEM 430) coupled with energy dispersive spectroscopy (EDS), respectively. Laser diffraction system (Better size 2000LD) was used for analyzing its size distribution. The micro-hardness was detected by HVS-1000 system using a load of 300 g for 15 s, the averaged microhardness was obtained from for 5 measurements points on the polished surface. Wear test was conducted on pin-on-disk system (SFT-2M). The wear conditions are as follows: applied load of 16 N, sliding time of 15 min, wear radius of 3 mm and sliding speed of 300 r/min. Prior to the wear test, the samples were polished and cleaned by alcohol. A 3D optical measurement system was applied to measure the cross-sectional of wear track. The wear rate was calculated as follows.

$$Q = V_w/FS \quad (2)$$

where Q is the wear rate in mm^3/Nm, V_w is the wear volume loss which can be derived from $2\pi rA$, A is the cross-sectional area of the wear track, r is the wear radius. N and S represent the applied load and the total sliding distance, respectively. In order to introduce macroscopic cracks and observe their propagation in the coating, the samples ($50\times20\times5$ mm^3) with section polished were used as for three-point bending (3PB) test by electronic universal testing machine (UTM5105). The load cell which pressed on the middle of the substrate moves down at a speed of 0.1 mm/min. The coating side was placed on two supporting points with an interval of 30 mm. The total distance in the whole test is 1.5 mm. Focused ion beam (FIB) technique was used to prepare TEM samples and observe deformation and cracking behaviors by transition electron microscope (TEM).

3. Results and discussion

3.1. Characterizations of powder

Fig. 2 shows the morphology, size distribution and phase of the as-atomized powder. It is observed that the powders were generally spherical and near-spherical shape, and limited satellite particles and dendritic structure as shown in Figs. 2a and b. The XRD pattern in Fig. 2c reveals that the powders were consists of cubic β-Al(Fe,Cu),τ-AlCu(Fe) and icosahedral QC (i-QC) phase, which is also reported in the melt-spun AlCuFe alloy system [17]. Fig. 2(d) displays a proper powder size distribution range of feedstocks for thermal spraying.

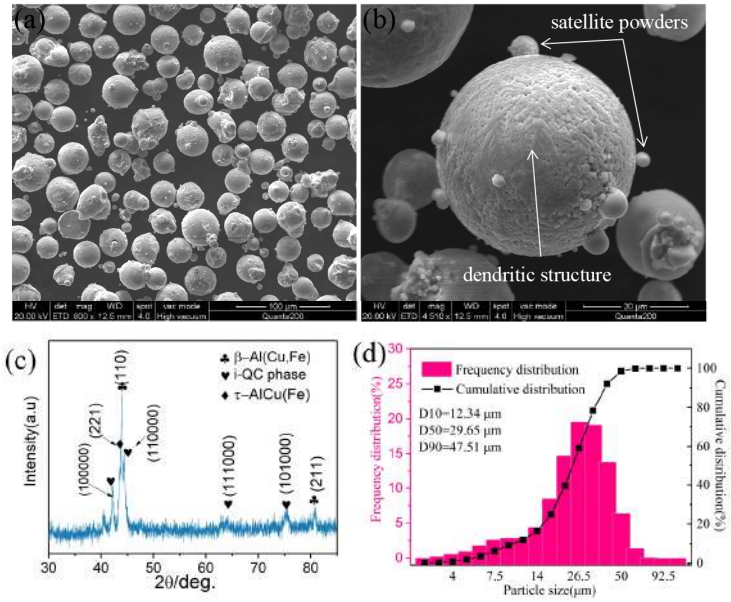

Fig. 2 Characterization of raw powders: (a) morphology, (b) enlarged particle showing the presence of dendrites, (c) XRD patterns, (d) powder size distribution

3.2. Orthogonal tests

Fig. 3 shows the XRD patterns of the HVAF sprayed coatings. It is clear that the coatings consisted of β-Al(Fe,Cu), τ-AlCu(Fe) and i-QC phase, consistent with that of raw powder shown in Fig. 2c. Due to the good control of particle size and the rapid cooling process of thermal spraying process, the major of feedstocks might have a partially melted state, which has a little effect on phase content.

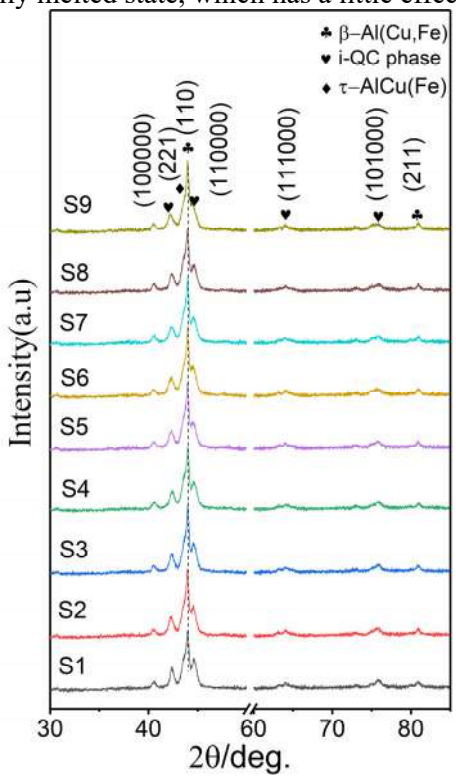

Fig. 3 XRD patterns of sprayed coatings with various conditions

The volume fraction of each phase area of the i-QC peaks (V_i) and β-Al(Fe,Cu) peak were measured based on XRD results as shown in Fig. 3(b) by using the following formula:

$$V_i = \frac{A_i}{A_i + A_\beta + A_\tau} \times 100\% \quad (3)$$

Where, A_i, A_β and A_τ are areas of i-QC， β-Al(Fe,Cu) and τ-AlCu(Fe) peaks, respectively. Table 1 shows the orthogonal test parameters, the results of microhardness tests and fraction of i-QC phases. It is noted that for different combination of spraying parameters, the coating microhardness and volume fraction of i-QC phase varied in a wide range of 468.4 - 580.5 $HV_{0.3}$ and 30.4 - 36.9%， respectively.

Table 1 Properties of Al-based coatings obtained based on orthogonal test

Sample No.	Factors			Results	
	A: Spray distance（mm）	B: Fuel 1 pressure （Mpa）	C: Feed rate （%）	Microhardness ($HV_{0.3}$)	Fraction of i-QC phase
S1	1（150）	1（0.63）	1（10）	517.5	36.52
S2	1	2（0.67）	2（20）	500.4	36.93
S3	1	3（0.72）	3（30）	561.5	35.84
S4	2（220）	1	2	516.0	34.62
S5	2	2	3	468.4	30.96
S6	2	3	1	580.5	32.40
S7	3（300）	1	3	525.5	31.64
S8	3	2	1	474.1	32.19
S9	3	3	2	517.5	30.41

To evaluate the importance order of these spraying parameters in sequence of microhardness and volume fraction of i-QC phases, the orthogonal analysis was introduced to calculate R values and the results were shown in table 2. Compared the R values for factors A(spray distance), B(fuel pressure) and C(feed rate), it can be concluded that the spraying parameters, affecting the coating microhardness, is in the order of B > A > C, the optimal spraying-parameter is B3A1C1, i.e. 0.72 Mpa, 150 mm, 10 g/min. Meanwhile, the spraying parameters, affecting the fraction of i-QC phases, is in the order of A ＞ B ＞ C. The optimal spraying-parameter is A1B1C2, i.e. 150 mm, 0.63 Mpa, 20 g/min. The fuel pressure decreased obviously from 0.74 Mpa to 0.63 Mpa in comparison with the optimal spraying parameters for microhardness.

Table 2 Range analysis of fraction of i-QC phases and microhardness of Al-based coatings obtained based on orthogonal test

		A: Spray distance （mm）	B: Fuel 1 pressure （Mpa）	C: Feed rate （g/min）
Range analysis of fraction of i-QC phases	K_1	109.29	102.78	101.11
	K_2	97.98	100.08	101.96
	K_3	94.24	98.65	98.44
	K_{AV1}	36.43	34.3	33.7
	K_{AV2}	32.66	33.98	34.0
	K_{AV3}	31.4	32.88	32.8
	R	5.03	1.4	1.2
	Optimal	A1	B1	C2
	Order		ABC	

Range analysis of microhardness	K_1	1578.4	1559.0	1572.1
	K_2	1564.9	1441.9	1532.9
	K_3	1517.1	1659.5	1555.4
	K_{AV1}	526.1	519.6	524.0
	K_{AV2}	521.6	480.6	510.9
	K_{AV3}	505.7	553.2	518.5
	R	20.4	72.6	13.1
	Optimal	A1	B3	C1
	Order	BAC		

(Note: for spray distance, K_1: 150 mm, K_2: 220 mm, K_3: 300 mm; for fuel pressure (1), K_1: 0.63 Mpa, K_2: 0.67 Mpa, K_3: 0.72 Mpa; for feed rate, K_1: 10 g/min, K_2: 20 g/min, K_3: 30g/min)

The average microhardness and the volume fraction of i-QC phases as a function of different factors are shown in Fig. 4. As the spray distance increased, both microhardness and fraction of i-QC phases show downward trend, exhibiting a positive correlation between these two parameters. For fuel pressure, the microhardness reaches the maximum value of 553.2 $HV_{0.3}$ and the minimum value of 480.6 $HV_{0.3}$ at the fuel pressure of 0.72 Mpa and 0.63 Mpa, respectively. Thus, the range R has the largest value of 72.6. For particle feed rate, with increasing feed rate, the microhardness decreases firstly and then increases. The value of microhardness fluctuated in a narrow range of 510.9 – 524.0 $HV_{0.3}$. The corresponding range R is 13.1, revealing the feed rate of powder has less effect on the micro hardness of quasicrystalline coatings compared with the other two factors. The volume fraction of i-QC phase is less sensitive to factors B and C compared with factor A, and its value maintains at around 34%. This result indicated that the micro hardness would be effectively tailored by factor B and C without considering the effect of the variation of fraction of i-QC phase. The feed rate of powder has less effect on volume fraction change of i-QC phase, which is consistent with its effect on the micro hardness.

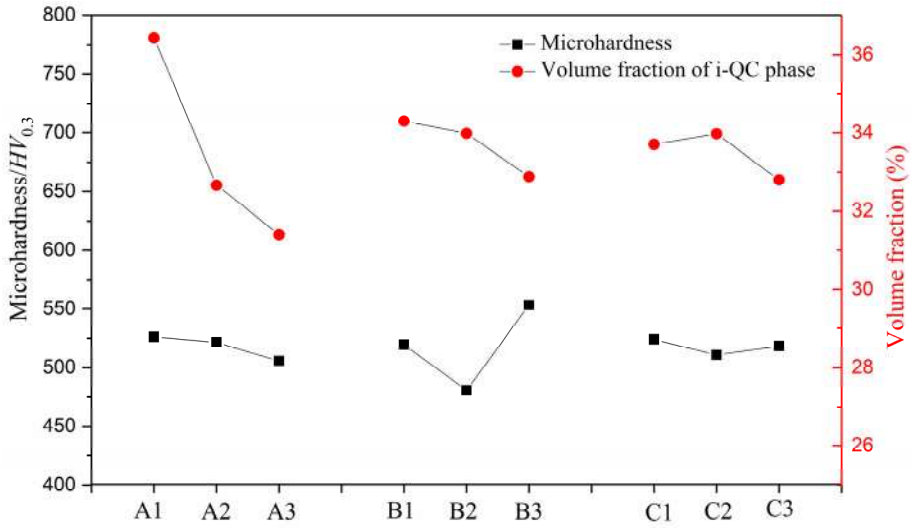

Fig. 4 Relationship between the factors, micro hardness and volume fraction of i-QC phases

Since the optimal spraying-parameters are not in 9 schemes of the designed orthogonal test. Instead,

the sample named S6 with the highest micro hardness in total 9 samples was prepared by parameters of A2B3C1. Hence, these levels which had the largest impact on three factors were assembled together to prepare a new sample for the confirmatory tests. This new sample was marked as S10. Table 3 summarized the spraying-parameters and micro hardness of Al-based quasicrystalline coatings. It can be seen that when the spray distance and fuel pressure are same, the highest hardness of 584.2 $HV_{0.3}$ is obtained by decreasing the spray distance from 220 to 150 mm.

Table 3 Summary of the processing parameters and microhardness of Al-based quasicrystalline coatings

Samples	Spray distance （mm）	Fuel 1pressure （Mpa）	Feed rate （g/min）	Microhardness （$HV_{0.3}$）
S5	220	0.67	30	468.4
S6	220	0.72	10	580.5
S10	150	0.72	10	584.2

3.3. Microstructure of the as-sprayed coatings

Apart from the inherent advantages including high hardness, low surface energy and enhanced ductile for good wear resistance, the microstructure of coating determined by spray process and the process parameters also plays an important role in coating properties and performance. Fig. 5 shows the morphologies of coating surfaces, cross-section and schematic diagram of microstructure evolution of S5 and S10. As shown in Fig. 5a and d, some un-melted particles with loose structure were observed on surface of S5. However, after optimizing the spray parameters, the un-melted particles disappeared and a number of smooth flattened splats could be observed on the surface of S10, indicating a better melting state of particles. As a result, cracks and large pores could be significantly inhibited and a dense microstructure was obtained (as shown in Fig. 5e). Fig. 5c and f show the schematic diagram of the microstructure evolution of the coatings S5 and S10 deposited by different spraying-parameters. The optimal spraying-parameters promote the sufficient deformation of the particles during impact on the substrate. These fine well-deformed splats lead to a better lamellar splat/splat contact and decrease of pores, suggesting a higher interfacial bonding between the splats. As a result, a fine-lamellar coating without big pores and obvious cracks was successfully prepared (as shown in Fig. 5f).

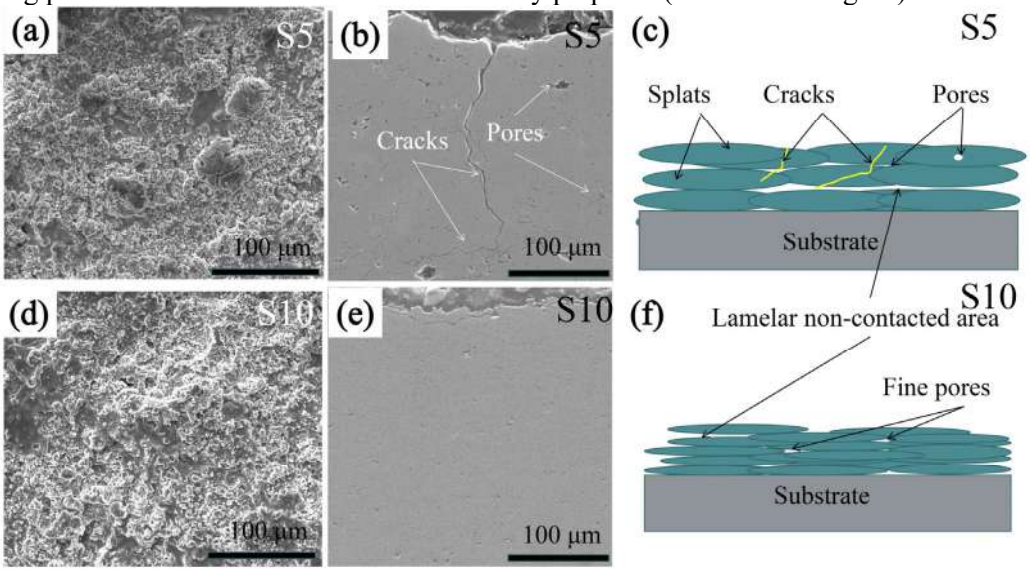

Fig. 5 The SEM morphologies of coating surfaces (a)(d), cross-section (b)(e) and schematic diagram describes the microstructure evolution

3.4. Tribological characterization and mechanical property

The tribological properties were evaluated by pin-on-disk configuration. The results are summarized in

Table 4. The friction coefficient (COF) value and wear rate of Al-based QC coating are around 0.45 and 3.1 $\times 10^{-4}$ $mm^3N^{-1}m^{-1}$, respectively. These two parameters of wear resistance are similar to that of spray forming of large volume Al-based composites reinforced with decagonal quasicrystals [18] , better than that of the Al-Si A380 material for the wear conditions applied [18]. Besides, it can be seen that the multi-phase quasicrystalline alloys (seen in Al+d-QC and Al+i-QC), containing a ductile phase and brittle phase, exhibits a better wear resistance in comparison with pure d-QC coatings. As reported by Lee. et al [1], multi-phase quasicrystalline alloys exhibit improved toughness and favorable crack resistance, together with a low friction provided by the i-phase and ductile phase, consequently, these alloys have a favorable wear and crack resistance. This provides a guideline for fabricating quasicrystal reinforced coatings and bulk components with increased wear resistance via spray-formed deposit, liquid solidification and powder metallurgy.

Table 4 Summary of the microhardness and wear properties of Al-based alloys

Alloy systems	Hardness (*HV*)	Friction coefficient (*COF*)	Wear rate ($\times 10^{-4}$ $mm^3.N^{-1}m^{-1}$)
Al-Si A380 [18]	110	0.55	7.7
Pure d-QC coatings [19]	755	0.58	13.5
Al+d-QC [18]	225	0.65	5.1
Al+i-QC (This work)	584.2	0.45	3.1

Note: d-QC and i-QC represent decagonal quasicrystals and icosahedral quasicrystals, respectively.

Fig. 6 shows the worn surface and the EDS spectrum acquired from the corresponding area. The worn track consists of white-contrast area and grey-contrast area, which are marked as point 1 and 2, respectively. The EDS spectrum of point 1 and 2 confirmed that the white-contrast area was unworn surface and grey-contrast area was worn area, respectively. The enlarged typical worn region was shown in fig. 6b. As can be seen, the worn area is found to be abrasive pit consisted of small peeled-off debris and cracks. An O concentration rich layer in upper left corner and a less Al concentration were observed from the EDS mapping, indicating partial construction of the debris film. Generally, localized wear takes place as cracking propagates from these abrasive wear pits with cracks and oxide formation. A large number of cracks initiate and rapidly expand along the vertical direction of the coating, and finally reach the interface between the coating and the substrate through defects such as pores and cracks which are unavoidable in coatings. Accompanying with the formation of a through-thickness cracking, the wear pits propagation leads to eventual failure of the coating. The worn morphology and EDS result revealed that the wear mechanism is abrasive wear together with oxidation wear.

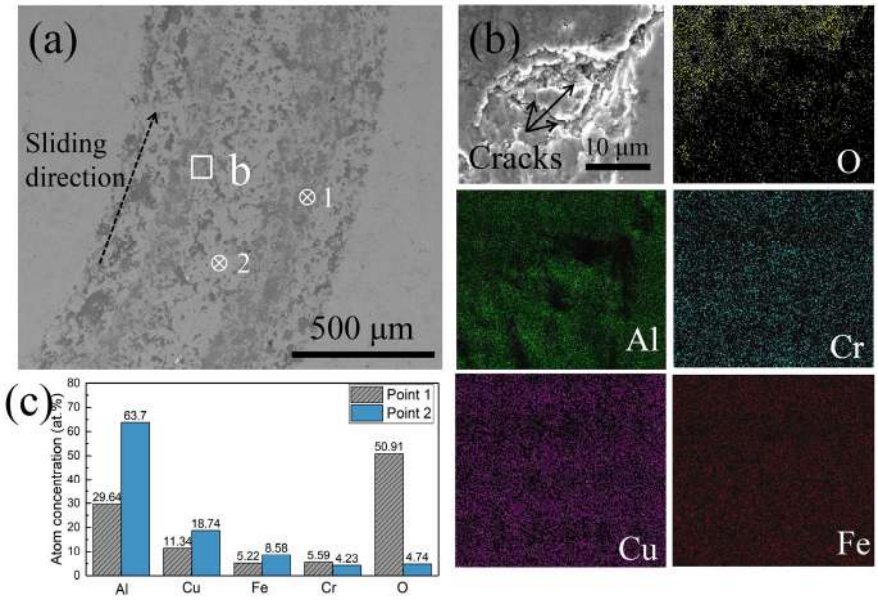

Fig. 6 Morphology of the wear track (a), EDS of oxide wear debris of point 1 (b) and friction coefficient (c)

Generally, because of the pinning of dislocation of quasicrystals [20], quasicrystals are harder than other aluminum alloys, which contributes to increase wear resistance , reduce the COF and the adhesive contribution on the COF values [21]. However, as the crack initiates, the integrity of the brittle coating was destroyed rapidly. Thus, the good crack tolerance plays an important role during the wear process. Fig. 7 shows the HAADF images and the corresponding EDS spectrum of the Al-based quasicrystal coating with cracks initiation. It can be seen that this coating consists Cu rich phase which was β-Al(Cu,Fe) phase, indicated by XRD result in Fig. 3a. As can be seen in HAADF image, the cracks penetrated through ductile Cu-rich phase and interrupted at inner pore. The inset is an enlarged image of selected area, shown in right corner of Fig. 7. As can be seen, the main crack initiated from the surface bypassed the black-contrast phase, forming more branched fine cracks within the white-contrast phase. Moreover, crack penetrated within the white-contrast phase and leaded to the exfoliation of a small piece of debris from the coating matrix. The above cracks propagation paths predominately go through the Cu rich phase and vanish at inter pores or formed more tiny branches. Due to the presence of ductile phase and/or micro pores, the internal stress at the crack tip is effectively released, and the multi-phase coating exhibits excellent both hardness and ductility. As a result, the Al-based quasicrystal coating has a favorable wear and crack resistance.

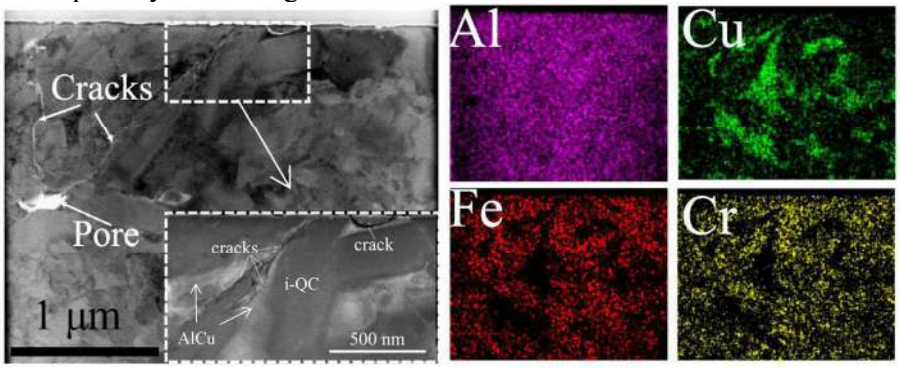

Fig. 7 HAADF images of crack initiation area and the corresponding EDS mapping

To further investigate the crack resistance of the coating, 3PB test was carried out at room temperature for S5 and S10. Fig. 8 shows the load-displacement curves of substrate, coating S5 and S10. The deformation process of the coating included three stages: 1) elastic deformation stage where

the stress was too low to destroy the coating; 2) crack propagation stage in which the substrate still underwent elastic deformation, however, a slow crack propagation process for coatings was triggered; 3) yield stage of the substrate and the crack propagation stage of the coating. Firstly, the deposited coatings improve the mechanical properties of the substrate in the 3PB test, among which, S10 exhibits the highest peak values of applied load in comparison with those of S5 and substrate at displacement of 1.5 mm. Secondly, in the crack growth stage (the second stage), the release of the stress caused by the micro-crack propagation results in the load–displacement curve of the coatings S5 and S10 below curve of the substrate. The load–displacement curve of S5 rapidly intersects with that of substrate, which was because of the coating fracturing quickly. Meanwhile, the stress of S10 increases more slowly with increasing displacement in comparison with that of S5, indicating a better crack tolerance characteristic. The stress accumulated in coating S10 was released smoothly in the second stage, indicating that the coating S10 had greater toughness.

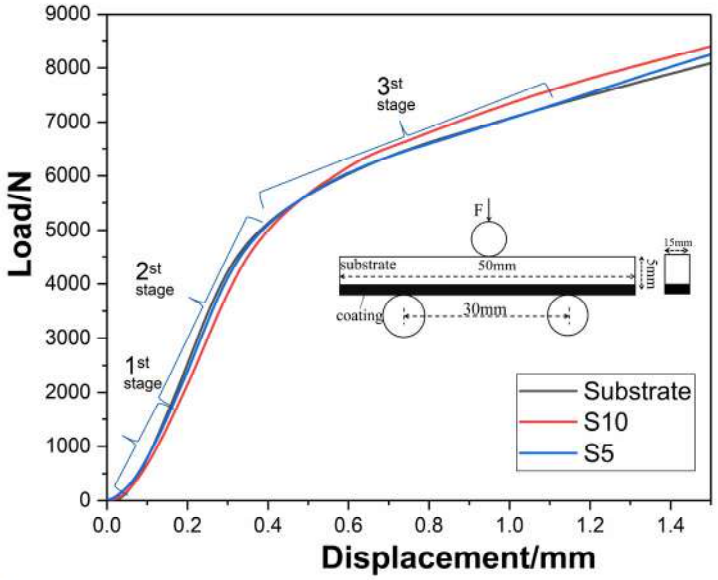

Fig. 8 Load–displacement curves of the coatings S5, S10 and substrate in 3 PB test

Fig. 9 shows the surface and cross-sectional morphology of the coatings after 3PB test. Figs. 9a and e show the optical images of the sample after 3PB test. A number of nearly parallel cracks can be observed in the middle of coatings, in which S10 prepared with optimal parameters (Fig. 9e) show more tiny cracks (marked by white dash box). As can be seen in Fig. 9b and f, the initiation and propagation of the micro cracks have a little difference. The cracks in S10 have obvious deflection and bifurcation, revealed by more tiny cracks appeared on coating surface. Fig. 9c and g show the cross-section view of the coatings, partial of the coating S5 was peeled off during the test. Because of the crack proliferation, the cracks interval reduced to a certain degree, thus, S10 shows a better integrity in comparison with S5. Fig. 9d shows the fracture morphology of S5. The tensile stress in the top layer resulted in the crack propagation along columnar interface, which reveals the typical brittle fracture mechanism. However， when the strain reached the interface between the splats, due to the pores and oxide inside the coating, the crack is prone to expand along the interface under the effect of shear stress. The crack propagation in S10 is prone to extend along the splats interface with a more horizontal direction (seen in Fig. 9h). The crack paths in S10 are discontinuous with several long plane crack interfaces formed. The coating exhibits two types of fracture behaviour: stepped brittle fracture and interlayer cracks propagation, indicating brittle fracture of the layer and crack propagation of the interlaminar.

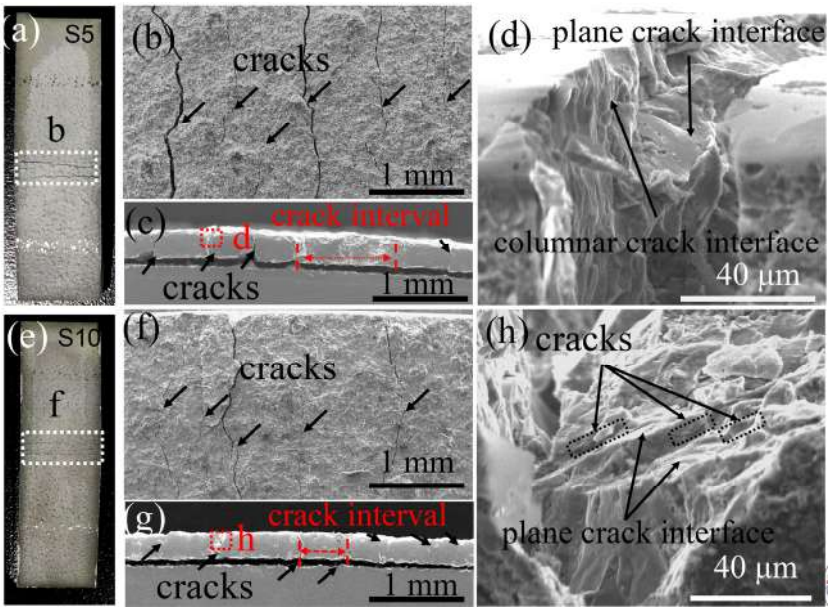

Fig. 9 OM images showing the sample surfaces after 3PB test (a)(e), local enlargement microstructure of middle region (b)(f), cross-sectional view of coatings (c)(g), magnified images of top crack regions of coatings (d)(h)

4. Conclusion

In this study, Al-based quasicrystalline coating with a high hardness of 584.2 $HV_{0.3}$ and a low porosity of 1.3% has been prepared successfully via HVAF process with optimizing the spraying parameters. The results suggested that the order that affects the microhardness is fuel pressure ＞ spray distance ＞ feed rate of powder, meanwhile, the order affected the fraction of i-QC phases is spray distance ＞ fuel pressure ＞ feed rate. The Al-based quasicrystalline coating exhibits a low wear rate of 3.1×10^{-4} $mm^3.N^{-1}m^{-1}$ and a low friction coefficient of 0.45. The good wear resistance originated from a finer lamellar and denser microstructure. Besides, the ductile phase in Al-based quasicrystalline coating also have a favorable wear and crack resistance, which provides an effective guideline in developing new wear resistance quasicrystalline coating. The dominating wear mechanism of Al-based quasicrystalline coatings is abrasive wear coupled with oxidation wear.

Acknowledgements

This work was supported by the National Natural Science Foundation of China (Grant No. 51901079), the Fundamental Research Funds for the Central Universities, the Opening Project of National Engineering Research Center for Powder Metallurgy of Titanium & Rare Metals, the Natural Science Foundation of Guangdong Province (No. 2018A030313615, 2018A030310406, 2020A1515010736), the Guangzhou Municipal Science and Technology Program (No. 202007020008), the Zhongshan Municipal Science and Technology Program (Platform Construction and innovation Team) (2016F2FC0005) and Zhongshan Collaborative Innovation Fund (2018C1001), Research and industrialization of key technologies of high-efficiency non-oriented electrical steel (191007102629094), Research and industrialization of key technologies of high-efficiency non-oriented electrical steel（191007102629094）.

References

[1] K. Lee, J. Hsu, D. Naugle, H. Liang, Multi-phase quasicrystalline alloys for superior wear resistance, Mater. Des, 108 (2016) 440-447.
[2] V.C. Srivastava, E. Huttunen-Saarivirta, C. Cui, V. Uhlenwinkel, A. Schulz, N.K. Mukhopadhyay, Bulk synthesis by spray forming of Al–Cu–Fe and Al–Cu–Fe–Sn alloys containing a

quasicrystalline phase, J. Alloys. Compd., 597 (2014) 258-268.
[3] M.F. P. Schall, K. Urban, Plastic deformation of decagonal Al–Ni–Co single quasicrystals, Mater. Sci. Eng A, 309–310 (2001) 548–551.
[4] Y. Zou, P. Kuczera, W. Steurer, R. Spolenak, Disappearance of plastic anisotropy in decagonal quasicrystals at small scales and room temperature, Extreme. Mech. Lett, 8 (2016) 229-234.
[5] R.Q. Guo, C. Zhang, Q. Chen, Y. Yang, N. Li, L. Liu, Study of structure and corrosion resistance of Fe-based amorphous coatings prepared by HVAF and HVOF, Corros. Sci, 53 (2011) 2351-2356.
[6] J. Wu, S.D. Zhang, W.H. Sun, J.Q. Wang, Influence of oxidation related structural defects on localized corrosion in HVAF-sprayed Fe-based metallic coatings, Surf. Coat. Technol., 335 (2018) 205-218.
[7] V. Matikainen, G. Bolelli, H. Koivuluoto, P. Sassatelli, L. Lusvarghi, P. Vuoristo, Sliding wear behaviour of HVOF and HVAF sprayed Cr3C2-based coatings, Wear, 388-389 (2017) 57-71.
[8] C. Zhang, R.Q. Guo, Y. Yang, Y. Wu, L. Liu, Influence of the size of spraying powders on the microstructure and corrosion resistance of Fe-based amorphous coating, Electrochim. Acta, 56 (2011) 6380-6388.
[9] H. Zhang, Y. Xie, L. Huang, S. Huang, X. Zheng, G. Chen, Effect of feedstock particle sizes on wear resistance of plasma sprayed Fe-based amorphous coatings, Surf. Coat. Technol., 258 (2014) 495-502.
[10] D.J. Sordelet, M.F. Besser, I.E. Anderson, Particle size effects on chemistry and structure of Al-Cu-Fe quasicrystalline coatings, J. Therm. Spray. Technol., 5 (1996) 161-174.
[11] T. Moskalewicz, B. Dubiel, B. Wendler, AlCuFe(Cr) and AlCoFeCr coatings for improvement of elevated temperature oxidation resistance of a near-α titanium alloy, Mater. Charact., 83 (2013) 161-169.
[12] D.J.Sordelet, M.F.Besser, J.L.Logsdon, Abrasive wear behavior of Al–Cu–Fe quasicrystalline composite coatings, Mater. Sci. Eng. A, 255 (1998) 54–65.
[13] L. Pawlowski, P. Fauchais, Thermal transport properties of thermally sprayed coatings, Int. Mater. Rev., 37 (2013) 271-289.
[14] L. Zhao, M. Maurer, F. Fischer, R. Dicks, E. Lugscheider, Influence of spray parameters on the particle in-flight properties and the properties of HVOF coating of WC-CoCr, Wear, 257 (2004) 41-46.
[15] Y. Bai, K. Liu, Z.H. Wen, J.J. Tang, L. Zhao, Z.H. Han, The influence of particle in-flight properties on the microstructure of coatings deposited by the supersonic atmospheric plasma spraying, Ceram. Int., 39 (2013) 8549-8553.
[16] M. Xiao, X. Liu, S. Zeng, Z. Zheng, G. Wang, Z. Qiu, M. Liu, D. Zeng, Effects of Particle Size on the Microstructure and Mechanical Properties of HVAF-Sprayed Al-Based Quasicrystalline Coatings, J. Therm. Spray. Technol., (2021).
[17] W. Wolf, F.G. Coury, M.J. Kaufman, C. Bolfarini, C.S. Kiminami, W.J. Botta, The formation of quasicrystals in Al-Cu-Fe-(M=Cr,Ni) melt-spun ribbons, J. Alloys. Compd., 731 (2018) 1288-1294.
[18] W. Wolf, L.P. M. e Silva, G. Zepon, C.S. Kiminami, C. Bolfarini, W.J. Botta, Single step fabrication by spray forming of large volume Al-based composites reinforced with quasicrystals, Scripta Mater., 181 (2020) 86-91.
[19] W. Wolf, G.Y. Koga, R. Schulz, S. Savoie, C.S. Kiminami, C. Bolfarini, W.J. Botta, Wear and Corrosion Performance of Al-Cu-Fe-(Cr) Quasicrystalline Coatings Produced by HVOF, J. Therm. Spray. Technol., 29 (2020) 1195–1207.
[20] D. Caillard, F. Mompiou, L. Bresson, D. Gratias, Dislocation climb in icosahedral quasicrystals, Scripta Mater., 49 (2003) 11-17.
[21] D.A. Rabson, Toward theories of friction and adhesion on quasicrystals, Prog. Surf. Sci., 87 (2012) 253-271.